Research Square

Preprints are preliminary reports that have not undergone peer review.
They should not be considered conclusive, used to inform clinical practice,
or referenced by the media as validated information.

A necrotrophy associated transcriptional profile of Thielaviopsis ethacetica during palm colonization

Sushmita Sapkota
University of Florida
Seemanti Chakrabarti
University of Florida
Navi Gill Dhillon
Nova Southeastern University
Madhugiri Nageswar-Rao
United States Department of Agriculture
Sukhwinder Singh
United States Department of Agriculture
Jeffrey A Rollins
University of Florida
Braham Dhillon
dhillonb@ufl.edu
University of Florida

Research Article

Keywords:

Posted Date: November 25th, 2026

DOI: https://doi.org/10.21203/rs.3.rs-11530549/v1

License: This work is licensed under a Creative Commons Attribution 4.0 International License.
Read Full License

Additional Declarations: No competing interests reported.

Abstract

Background

Thielaviopsis ethacetica is a soilborne fungal pathogen that causes trunk rot of palms and is the predominant member of the *T. paradoxa* species complex in Florida. This pathogen can colonize all major palm tissues, but successful infection requires mechanical wounding to enable fungal entry. Inoculation of wounded leaflets results in lesion development within three days post-inoculation. Although the basic infection biology of *T. ethacetica* has been described, the molecular mechanisms that underlie its ability to colonize palm tissues remain unknown.

Results

RNAseq was performed at 0 (T1), 24 (T2), and 48 (T3) hours post inoculation (hpi) to characterize the transcriptional response of *T. ethacetica* during palm colonization. Temporal expression patterns revealed a distinct transcriptional profile at T1 (0 hpi) and greater overlap between T2 (24 hpi) and T3 (48 hpi), while GO enrichment at T3 indicated increased representation of translation, ribosome biogenesis, and carbohydrate metabolic processes among upregulated genes. At T3, 1,202 genes were differentially expressed relative to control, including 303 upregulated and 899 downregulated genes. Upregulated genes included those involved in plant cell wall degradation, carbohydrate transport and downstream carbon metabolism. This was accompanied by upregulation of auxiliary activity enzymes and redox associated proteins, consistent with their roles in oxidative substrate degradation and maintenance of cellular redox homeostasis. Genes involved in proteolysis, amino acid transport and metabolism, as well as iron and phosphorus acquisition were also upregulated, suggesting active utilization of host derived nutrients. Genes associated with translation and ribosomes comprised the largest upregulated functional category. Concurrent upregulation of genes involved in fungal cell wall remodeling, translation and ribosome function was consistent with increased biosynthetic activity and fungal growth. Among the upregulated genes at T3, 23 candidate effectors, including BAS2, NPP1, and GH28 were identified. Three uncharacterized DUF7029 domain containing proteins ranked among the five most highly upregulated genes at T3. Additionally, a set of five collinear genes, putatively encoding an isocyanide biosynthetic pathway, were coordinately upregulated.

Conclusions

The strong upregulation of CAZymes, a gene cluster, putative effectors including the NPP proteins, highlights previously uncharacterized components of the *T. ethacetica* infection response. Collectively, these findings implicate processes involved in host cell wall degradation, nutrient utilization, and fungal growth, revealing a transcriptional response consistent with necrotrophic mode of colonization.

Introduction

Thielaviopsis ethacetica, a member of the *T. paradoxa* species complex, is a soilborne pathogen associated with diseases of several economically important crops, including palms, sugarcane, pineapple, banana, cacao, and bell pepper [1–5]. In palms, *Thielaviopsis* spp. can cause trunk and heart (bud) rot, posing a serious threat to landscape palms and commercial plantations in tropical and arid regions worldwide. In landscape palms, disease symptoms often manifest in the canopy or upper third of the trunk, suggesting that the pathogen may be introduced through fresh pruning wounds by contaminated pruning tools. *Thielaviopsis ethacetica* can colonize multiple palm tissues, including roots, trunks, fruits, and leaves [6], although infection requires mechanical wounding [7]. In both sugarcane and palm trunks, the pathogen can cause extensive damage to pith parenchyma cells, leaving the vascular bundle fibers largely intact [6, 8]. As trunk rot progresses, the resulting tissue degradation can compromise structural integrity, eventually leading to trunk or canopy failure [7].

Recent studies identified *T. ethacetica* and an undescribed *Thielaviopsis* species as causal agents of palm trunk rot in Florida, with *T. ethacetica* identified as the predominant species [9]. These two species differ in virulence, thermotolerance, fungicide response, morphology and growth characteristics [9]. Despite its importance, studying host pathogen interactions in palms is challenging as whole plant inoculation studies are labor intensive and difficult to conduct in long-lived woody perennials. As such, the molecular mechanisms underlying *T. ethacetica* colonization of palm tissues remain poorly understood. In particular, the fungal genes and pathways involved in its interaction with palm tissues have not yet been characterized. To address these challenges, a detached leaf assay was previously developed to facilitate rapid screening for host resistance to *Thielaviopsis*, with inoculation of wounded palm leaflets producing visible lesions within three days post inoculation [10]. Although originally developed for resistance screening, this detached leaf assay also provides a controlled experimental system for studying *T. ethacetica* - palm interactions.

In this study, detached leaf assay coupled with RNA sequencing was used to characterize transcriptional changes in *T. ethacetica* during interaction with foxtail palm leaflets at 0, 24, and 48 hours post inoculation (hpi). Fungal gene expression during host interaction was compared with that during axenic growth, and differentially expressed genes were examined, with particular emphasis on pathogenicity associated functions, including carbohydrate-active enzymes (CAZymes), effectors, proteases, and transporters. Transcriptomic analysis revealed increased expression of genes associated with plant cell wall degradation, nutrient acquisition, and fungal growth at 48 hpi. The analysis also identified strongly upregulated candidate pathogenicity associated genes, including predicted secreted proteins and previously uncharacterized proteins, providing new insights into the molecular processes associated with *T. ethacetica* - palm interactions.

Materials & Methods

Pathogen inoculation, sample collection and RNA extraction

Detached leaflets of foxtail palm were inoculated with spore suspension of *Thielaviopsis ethacetica* isolate TP_5448A [10] (Supp. Figure S1). Leaflets were mechanically punctured prior to inoculation using a custom tool with six needles arranged in a hexagon pattern. A total of 10 µl of spore suspension (1×10^6 spores/ml) was applied to each wounded site, while fungal tissue collected from 0.5x potato dextrose agar served as control material. Leaflets were placed in 100 mm glass Petri plates lined with sterile, moist filter paper and incubated at 28°C in the dark. Leaf samples were collected at 0 (T1), 24 (T2), and 48 (T3) hours post-inoculation (hpi), and fungal tissue was harvested from culture plates at 48 hpi (T4). Hence, a total of four treatments, with three independent biological replicates were prepared. The total RNA was extracted using TRIzol (ThermoFisher Cat #15596018) following the manufacturer's instructions. RNA concentration and quality were assessed using a 5300 Fragment Analyzer (Agilent, Santa Clara, CA, USA) and all RNA samples were sequenced at The DNA Sequencing Lab, Roy J. Carver Biotechnology Center, University of Illinois at Urbana-Champaign on the Illumina Novaseq X series platform using 2 × 150 bp paired-end sequencing.

RNAseq data processing and differential expression analysis

The quality of raw reads was first assessed using FastQC v0.12.1 [11]. Raw FASTQ files were filtered with fastp v0.23.4 [12], and reads shorter than 80 bp or with Phred quality score < 20 were discarded and adapter sequences were removed. The resulting high quality reads were mapped to the *Thielaviopsis ethacetica* reference genome using the splice aware aligner HISAT2 v2.2.1-3 [13]. Alignment files in SAM format were converted to sorted BAM files with SAMtools v.1.20 [14]. Gene expression levels were quantified from the aligned reads using StringTie v2.2.3 [15]. Gene- and transcript-level count matrices were generated using the prepDE.py3 script provided with StringTie and used as input for differential expression analysis in R v4.5.1 (2025-06-13, "Great Square Root") [16] using package DESeq2 v1.50.2 [17]. Differentially expressed genes (DEGs) were identified using thresholds of *P*adj ≤ 0.05 and absolute |log2 fold change| ≥ 2. Data filtering and visualization was performed in R using tidyr v1.3.1 [18], dplyr v1.1.4 [19], ggplot2 v3.5.2 [20], ggtext v.0.2.0 [21], and ggrepel v0.9.6 [22], including volcano plots, principal component analysis (PCA). For PCA, the normalized expression data were transformed using the variance stabilizing transformation (vst) implemented in DESeq2. The R package pheatmap v1.0.13 [23] was used to generate the heatmaps.

GO enrichment analysis and temporal expression profiling

Gene Ontology (GO) enrichment was performed using the R package clusterProfiler v4.16.0 [24]. Duplicate gene-GO associations were removed prior to analysis, and over-representation analysis was conducted with the enricher function using all genes with available GO annotations as the background. Significantly enriched GO terms were identified using Benjamini-Hochberg correction, with *P*adj and *q* values ≤ 0.05 considered significant. GO term names, ontology classifications, and definitions were retrieved from the EMBL-EBI QuickGO database using httr v1.4.9 [25] and jsonlite v2.0.0 [26]. Upregulated genes (*P*adj ≤ 0.05 and log2FC ≥ 2) were classified at each time point resulting in seven

temporal expression patterns, T1-specific, T2-specific, T3-specific, T1 + T2, T1 + T3, T2 + T3, and T1 + T2+T3. Expression patterns were visualized in R across three time points (T1, 0 hpi; T2, 24 hpi; and T3, 48 hpi) by plotting individual gene log2 fold-change trajectories together with the mean trajectory for each pattern.

Results

Transcriptomic response of Thielaviopsis ethacetica during colonization of palm leaves

Transcriptomic analysis of the interaction between *Thielaviopsis ethacetica* and foxtail palm (*Wodyetia bifurcata*) was conducted at three stages of infection, T1 (0 hpi; ungerminated spores), T2 (24 hpi; early germination and host colonization), and T3 (48 hpi; active necrotic lesion formation), with *T. ethacetica* mycelia grown *in vitro* for 48 h (T4) used as the reference condition. Across the four treatments, an average of 171 million reads was generated per biological replicate, resulting in ~ 2 billion reads in total (Table 1). Principal component analysis (PCA) showed that the first two principal components explained 87% of the total variance and clearly separated the treatments. T2 and T3 exhibited greater transcriptomic similarity, whereas T1 and T4 were distinctly separated from these treatments and each other, with replicates clustering tightly within each treatment (Fig. 1). Comparison of each infection stage with the T4 reference identified 4,305, 2,146, and 1,202 differentially expressed genes (DEGs; $|\log2FC| \geq 2$; $Padj \leq 0.05$) at T1 (0 hpi), T2 (24 hpi), and T3 (48 hpi), respectively (Fig. 2; Supp. Fig. S2). Of these, 219, 249, and 303 genes were upregulated, whereas 4,086, 1,897, and 899 genes were downregulated at T1, T2, and T3, respectively (Supp. Table S1-S3).

Table 1
Summary of sequencing read counts and mapping statistics for *Thielaviopsis ethacetica* samples.

Sample*	Total Reads	Mapped Reads	Percent Mapped (%)
0 hpi (T1_R1)	176,734,545	352,751	0.2
0 hpi (T1_R2)	181,843,514	595,852	0.33
0 hpi (T1_R3)	159,568,228	677,419	0.42
24 hpi (T2_R1)	159,953,814	1,162,047	0.73
24 hpi (T2_R2)	179,553,854	1,711,920	0.95
24 hpi (T2_R3)	194,766,850	1,168,496	0.6
48 hpi (T3_R1)	194,565,890	12,860,660	6.61
48 hpi (T3_R2)	191,359,623	21,985,124	11.49
48 hpi (T3_R3)	195,379,634	15,604,766	7.99
Control (T4_R1)	135,368,813	127,513,389	94.2
Control (T4_R2)	145,891,059	138,037,301	94.62
Control (T4_R3)	136,753,297	127,163,496	92.99
*hpi: hours post inoculation			

Temporal expression patterns

The upregulated genes displayed distinct temporal expression patterns across the three *in planta* time points (Fig. 3; Supp Table S4). Individual stage specific upregulated genes were identified at all three time points, T1, T2, and T3, with 153, 53, and 109 genes, respectively, while additional genes were shared across time points. The largest shared group comprised 135 genes upregulated at both T2 and T3, whereas relatively few genes were shared between T1 and T2 (7 genes) or T1 and T3 (5 genes). A smaller core of 54 genes was upregulated at all three time points. Thus, although each stage included a distinct set of upregulated genes, the expression patterns at 24 hpi (T2) and 48 hpi (T3) showed substantially greater overlap than either timepoint did with 0 hpi (T1).

Classification of the upregulated DEGs into clusters of orthologous groups (COG) categories provided a broad functional overview of the temporal expression patterns. COG assignments were available for 359 of the 515 upregulated genes with 156 lacking an assigned category (Supp. Table S5). The COG category 'translation, ribosomal structure and biogenesis' occurred across multiple expression patterns, including 43 genes upregulated at all three time points, 26 genes shared between T2 and T3, and 20 genes specific to T1. The T1-specific group also showed substantial representation of the COG category 'RNA

processing and modification' (31 genes). In contrast, the COG categories 'carbohydrate transport and metabolism' and 'posttranslational modification and protein turnover' were prominent among genes shared between T2 and T3 (21 and 16 genes, respectively) and among T3-specific genes (18 and 15 genes, respectively). Two additional COG categories 'amino acid transport and metabolism' and 'secondary metabolite biosynthesis, transport and catabolism' were represented at lower levels but occurred consistently among the T1-, T2-, and T3-specific upregulated DEGs.

Enrichment analysis

GO enrichment analysis revealed distinct profiles among the upregulated and downregulated DEGs at T3 relative to T4, the *in vitro* reference (Fig. 4). The upregulated DEGs were characterized by particularly strong enrichment of translation and ribosome related processes, with fold enrichment reaching up to 16-fold, whereas the downregulated DEGs showed more moderate enrichment, generally below 5-fold, in processes related to morphogenesis and carbohydrate metabolism. The two DEG sets therefore differed not only in the biological processes represented but also in the magnitude of their overrepresentation.

Among the 260 downregulated DEGs with GO annotations, enriched terms were primarily associated with growth, morphogenesis, sporulation, cell wall organization, and carbohydrate metabolism. Growth related GO terms included growth, regulation of growth, and regulation of filamentous growth, while morphogenesis and sporulation terms were also overrepresented. Carbohydrate metabolism included broader carbohydrate metabolic processes as well as more specific processes involving carbohydrate derivatives, aminoglycans, amino sugars, and chitin. Cell wall organization or biogenesis was also enriched, while antibiotic catabolism and neutral lipid metabolism represented additional, more limited enrichments.

Among the 135 upregulated DEGs with GO annotations, the most extensive enrichment was associated with three GO categories, namely, ribosome biogenesis, rRNA processing, and translation, encompassing processes involved in ribosome assembly and maturation as well as cytoplasmic and mitochondrial protein synthesis. The GO categories peptide metabolic and biosynthetic processes were also strongly overrepresented, with approximately 7- to 8-fold enrichment. Enrichment of nucleic acid transport included RNA and rRNA transport and nuclear export, while organelle assembly was also overrepresented. Carbohydrate related processes were represented by enrichment of polysaccharide metabolic and catabolic processes as well as broader carbohydrate metabolism and catabolism. The upregulated DEGs at T3 were further examined to characterize their functional classes, predicted activities, and patterns of coordinated expression.

Coordinated upregulation of plant cell wall degrading enzymes

A dominant feature of the *T. ethacetica* transcriptional response at 48 hpi (T3) was the upregulation of genes encoding carbohydrate active enzymes (CAZymes) involved in degradation and modification of plant cell wall polysaccharides (Fig. 5A). In total, 44 upregulated DEGs were assigned to the COG

category ‘carbohydrate transport and metabolism’, comprising an extensive repertoire of CAZymes targeting cellulose, hemicellulose, pectin, and other polysaccharides. These included genes from 18 families of glycoside hydrolases, GH1, GH2, GH3, GH5, GH7, GH10, GH11, GH16, GH18, GH28, GH30, GH32, GH43, GH45, GH51, GH61/AA9, GH74, and GH131, together with carbohydrate binding modules (CBM), carbohydrate esterases (CE), and polysaccharide lyases (PL).

The strongest upregulation occurred among several extracellular hydrolases. A galactosidase gene (GH16; gene_02455) showed a log2FC of 8.58 (padj = 2.10E-62), while an endopolygalacturonase gene (GH28; gene_01971) was strongly upregulated (log2FC = 7.70; padj = 1.50E-105). Cellulose directed activity was mediated by GH5, GH7, and GH61/AA9 genes, while pectin degradation enzymes included endopolygalacturonase GH28, pectin esterase CE8, and polysaccharide lyases PL1 and PL4. Xylan degradation was associated with multiple GH10 genes (gene_07251, gene_06458) and a GH11 gene (gene_03295).

The catalytic domains of the upregulated glycosyl hydrolases were frequently associated with carbohydrate binding modules (CBMs), particularly the fungal associated CBM1 domain. Among the upregulated CAZymes containing CBMs, CBM1 was the most prevalent domain occurring in 19 proteins, whereas CBM4 and CBM91 were each represented once. CBM63 occurred in two proteins as a standalone carbohydrate binding module. CBM1 and CBM63 are primarily associated with cellulose binding, while CBM4 is associated with crystalline cellulose binding and CBM91 is associated with xylan binding.

Several genes associated with carbohydrate uptake were also upregulated. These included three major facilitator superfamily (MFS) transporter genes (gene_04122, gene_04416, gene_04276), and three genes annotated as sugar transporters (gene_07302, gene_00184, gene_00678).

Oxidative enzymes and carbon substrate metabolism

In addition to the hydrolytic CAZymes, multiple auxiliary activity (AA) enzymes and oxidoreductases were upregulated. Upregulated genes included AA7, AA8, AA16, FAD monooxygenases, FMN-dependent dehydrogenases, and other flavin-dependent oxidoreductases (Fig. 5A). An AA7 oxidoreductase (gene_02883) was among the most strongly upregulated genes in the dataset (log2FC = 7.89; padj = 6.64E-102), while a AA8-CBM1 protein (gene_05824) showed a log2FC of 8.78 (padj = 3.20E-114). An additional AA8 protein (gene_06433), annotated as a cellobiose-dehydrogenase protein, was also strongly upregulated (log2FC = 6.14).

The response also included several enzymes involved in dehydrogenation and reduction reactions associated with carbon metabolism. An FMN-dependent dehydrogenase (gene_02949; log2FC = 5.84; padj = 7.63E-59) was strongly upregulated together with an aldehyde dehydrogenase (gene_03016; log2FC = 5.95; padj = 0.011). Several aldo-keto reductases were also upregulated, including a Xyl1/aldo-

keto reductase (gene_03457) that showed strong upregulation (log2FC = 5.69; padj = 9.48E-12), and several aldo-keto reductases (gene_04852, gene_03457, gene_06052, gene_06645, and gene_00992).

Additional upregulated genes were associated with downstream carbon metabolism and utilization, including a galactose mutarotase-like domain containing protein, galactokinase, enolase, and triosephosphate isomerase. Other metabolic enzymes included lactoylglutathione lyase, NAD-dependent oxidoreductases, and tannase.

Several additional upregulated genes were annotated with functions associated with secondary metabolism and redox-dependent reactions, including short-chain dehydrogenase/reductases (gene_01672, gene_04136), carotenoid cleavage oxygenase (gene_02476), Cu amine oxidase (gene_05573), 3-oxoacyl-acyl carrier protein reductase (gene_02553), and an alcohol dehydrogenase (gene_01748). An ABC transporter (gene_05261) and 2-deoxy-D-gluconate 3-dehydrogenase (gene_06050) were also upregulated.

Notably, five strongly upregulated genes occurred in a collinear genomic region comprising an MFS transporter (gene_04122; log2FC = 6.26; padj = 1.59E-10), an FAD monooxygenase (gene_04123; log2FC = 6.69; padj = 8.98E-58), an isocyanide-dioxygenase (DIT1-TauD; gene_04124; log2FC = 6.65; padj = 1.23E-7), and two CAZymes, a AA9 + CBM1 protein (gene_04126; log2FC = 6.90; padj = 3.11E-83) and a GH74 + CBM1 protein (gene_04128; log2FC = 5.25; padj = 8.13E-42). These genes were co-expressed and occurred within the same genomic region, indicating coordinated transcription of transporter, oxidoreductase, dioxygenase, and carbohydrate active enzyme functions.

Upregulation of antioxidant and redox-associated genes

Genes associated with antioxidant activity and cellular redox homeostasis were also upregulated. These included class II peroxidase (AA2; gene_00984; log2FC of 5.87; padj = 9.24E-68), mitochondrial peroxiredoxin (gene_04412), redoxin (gene_00306), glutathione S-transferase (gene_01528). Additional redox associated responses included NADH flavin oxidoreductase (gene_01310), a strongly upregulated FAD monooxygenase (log2FC = 6.69; padj = 8.98E-58), and the aldo-keto reductases mentioned above. The previously described AA7 and AA8 enzymes may also contribute to the broader oxidative enzyme response.

Additional redox-associated proteins included two cupredoxin-containing proteins and an RmlC-like cupin, further expanding the set of upregulated proteins with putative redox-associated functions.

Fungal cell wall remodeling and growth

Genes associated with fungal cell wall organization and remodeling were upregulated at 48 hpi, including a GH18 glycoside hydrolase/chitinase (gene_06914) that showed strong upregulation (log2FC = 8.43; padj = 6.48E-155), a strongly upregulated Mid2-like cell wall stress sensor (gene_03168; log2FC = 5.07; padj = 1.12E-169), and a glycosyltransferase GT4 (gene_06575) associated with fungal cell wall integrity and cell wall/membrane biogenesis.

Similarly, genes assigned to COG category 'translation, ribosomal structure and biogenesis' were also upregulated. This category comprised of 78 genes, representing the largest functional category in the dataset. This includes numerous 40S and 60S ribosomal proteins, translation factors, and aminoacyl-tRNA synthetases that were coordinately upregulated. Ribosomal protein S27a (gene_02915) had a log2FC of 2.52 (padj = 1.47E-273), while translation elongation factor eEF-1 gamma (gene_04813) showed a log2FC of 2.49 (padj = 4.13E-180). Additional upregulated translation-associated genes included mitochondrial elongation factor G (EF-Gmt), Translation elongation factor Tu (EF-Tu), and several aminoacyl-tRNA synthetases (gene_01332, gene_01733, gene_01847).

Proteolysis and acquisition of additional nutrient sources

In addition to carbohydrate degradation, *T. ethacetica* upregulated a broad repertoire of proteolytic enzymes (Fig. 5B). Thirty-four genes were assigned to the COG category 'posttranslational modification, protein turnover, and chaperones', including multiple peptidase families, A1, S8, M36, M1, M3, M24B, M28, M48, and M49, that were upregulated. Several proteases were among the most highly upregulated genes, including peptidase A1 genes, gene_06849 (log2FC = 8.17; padj = 1.51E-170) and gene_00804 (log2FC = 7.03; padj = 2.11E-51), as well as M36 metalloproteases, gene_01968 (log2FC = 5.88; padj = 2.46E-5) and gene_05881 (log2FC = 5.15; padj = 2.90E-28). Additional upregulated proteases included peptidase S8 genes gene_00989 (log2FC = 7.25; padj = 0.0071) and gene_06736 (log2FC = 3.05; padj = 1.93E-16), and peptidase A4 gene_02608 (log2FC = 6.04; padj = 1.18E-63).

Genes associated with amino acid transport and metabolism were also upregulated. These included an L-amino-acid oxidase (gene_01643, log2FC = 5.64; padj = 2.91E-5), two taurine catabolism dioxygenases, gene_04124 (log2FC = 6.65; padj = 1.23E-7) and gene_04377 (log2FC = 2.68; padj = 5.37E-13), a methionine synthase (gene_01635, log2FC = 2.93; padj = 4.10E-10), and additional aminotransferase and amino-acid metabolic enzymes. Three OPT-family oligopeptide transporters (gene_02479, gene_03873, gene_04730) was also upregulated.

Genes associated with sulfur metabolism were also represented among the upregulated transcripts, including two sulfite reductase genes (gene_02223, gene_04261), methionine synthase (gene_01635) and two taurine catabolism dioxygenases (gene_04124, gene_04377).

Acquisition and management of inorganic nutrients

The response included genes associated with acquisition, storage, and mobilization of inorganic nutrients. Iron-associated genes included ferric reductase, ferritin, VIT1, and CFEM-domain proteins. Ferritin (gene_01826) was strongly upregulated (log2FC = 5.64; padj = 7.79E-100), while the ferric reductase-like gene gene_01383 showed a log2FC of 5.44 (padj = 1.27E-7). Two CFEM-domain proteins, gene_02882 (log2FC = 7.48; padj = 1.26E-11) and gene_01520 (log2FC = 2.36; padj = 2.82E-19), were also upregulated, along with the vacuolar iron transporter VIT1 gene (gene_05218).

Phosphorus-associated functions included three histidine acid phosphatase (phytase) genes, gene_03692 (log2FC = 3.46; padj = 7.15E-45), gene_01159 (log2FC = 5.40; padj = 7.81E-5), and

gene_04946 (log2FC = 2.69; padj = 1.45E-30). Additional upregulated phosphatase-associated genes included a phosphoesterase (gene_05217; log2FC = 4.89; padj = 3.92E-15), and a glycerophosphoryl diester phosphodiesterase (gene_04397; log2FC = 4.72; padj = 1.62E-15).

Effectors, secreted proteins and highly upregulated uncharacterized genes

Among the upregulated genes, 101 encoded proteins had predicted secretion signals, including 23 classified as effectors (Fig. 5C). Seventeen of these putative effectors had functional annotations, including nine associated with carbohydrate binding or degradation described above, endopolygalacturonase GH28 (gene_01971), GH11 + CBM1 (gene_03295, gene_01447), GH131 (gene_00971), GH7 + CBM1 (gene_02417), CBM1 (gene_01079), pectate lyase PL1 (gene_06937), polysaccharide deacetylase (gene_00238), and cellobiose dehydrogenase AA8 (gene_06433). The remaining eight annotated effectors were fungal toxin *Alternaria alternata* allergen 1-like (Alt a1; gene_06003), two NPP1 necrosis-inducing proteins (gene_01240, gene_02169), biotrophy-associated secreted protein 2 (BAS2; gene_01766), cutinase CE5 + CBM1 (gene_06676), ribosomal protein S17 (gene_03630), and proteins containing domains DUF3129 (gene_02343) and DUF7143 (gene_01597). Among these, NPP1 (gene_01240; log2FC = 7.68; padj = 4.68E-10), DUF3129 (gene_02343; log2FC = 6.84; padj = 5.19E-152), and BAS2 (gene_01766; log2FC = 5.65; padj = 6.23E-12) showed strong upregulation.

The remaining six upregulated effector genes lacked functional annotation, including, gene_00991 (110 aa), gene_05444 (122 aa), gene_07033 (83 aa), gene_03762 (231 aa), gene_03697 (85 aa), and gene_00763 (203 aa). These included three strongly upregulated genes, gene_00991 (log2FC = 6.78; padj = 4.07E-122), gene_05444 (log2FC = 6.50; padj = 9.41E-27), and gene_07033 (log2FC = 5.84; padj = 1.07E-90).

Among proteins with predicted secretion signals, three proteins containing DUF7029 domain (gene_06449, gene_02445, and gene_05929) represented another group of strongly upregulated genes. When the upregulated genes were ordered by decreasing log2FC, these genes occupied three of the top five positions, with log2FC values of 9.44, 9.35, and 8.65, respectively. Another upregulated secreted protein was annotated as a Jacalin-type lectin domain containing protein (gene_04830).

Across the complete set of upregulated genes, 18 genes with predicted secretion signals lacked functional annotation, whereas several additional highly upregulated genes lacked both informative functional annotation and predicted secretion signals. These included gene_06103 (log2FC = 9.45; padj = 0.042), gene_04675 (log2FC = 7.20; padj = 0.0030), gene_00904 (log2FC = 6.98; padj = 5.21E-16), and gene_02925 (log2FC = 3.19; padj = 0.0049).

Discussion

This study provides insights into the transcriptional response of *T. ethacetica* during palm interaction and identifies candidate genes potentially involved in host colonization. The differentially expressed genes at

48 hours post inoculation span several functional categories, including nutrient acquisition (CAZymes, proteases, and transporters), host defense modulation (putative effectors), and fungal growth and development (chitinases, translation machinery, and ribosome biogenesis). Collectively, this *in planta* transcriptional reprogramming in *T. ethacetica* is consistent with the varied strategies characteristic of necrotrophic fungi.

The transcriptomic profiles reveal a marked transition from an early stage transcriptional state (T1) to active host associated growth (T2, T3). The strong separation of T1 from the *in planta* samples was consistent with the predominantly ungerminated spores and limited fungal biomass at this stage. In contrast, the closer clustering of T2 and T3 in the PCA, together with their substantial overlap in the temporal pattern of upregulated genes, supports continuity of the transcriptional program during host colonization as fungal biomass increases and lesions develop. T3 nevertheless represents a more advanced stage, with extensive necrotic lesion formation and additional stage-specific responses. The 153 T1-specific upregulated genes also indicate that the spore stage is transcriptionally active and may involve a distinct developmental program. Increasing the sequencing depth and number of sampled time points would help resolve these early responses and the transition from initial colonization to full lesion development.

The downregulated genes at T3 relative to T4 are reciprocally upregulated at T4 as compared to T3. These genes are enriched for terms related to growth, morphogenesis, sporulation, cell wall organization, and carbohydrate metabolism. The enrichment of these terms at T4 is consistent with vegetative growth under nutrient rich *in vitro* conditions, whereas *in planta* growth is associated with increased expression of genes involved in translation, proteolysis, nutrient acquisition, carbohydrate degradation, and cell wall remodeling. Together, these contrasting enrichment patterns indicate a shift in the cellular processes supporting fungal growth *in planta* rather than a reduction in fungal growth.

The upregulation of a broad set of plant cell wall degrading enzymes suggests extensive remodeling of the host cell wall during *T. ethacetica* colonization. Glycosyl hydrolases (GH) and auxiliary activity (AA) enzymes contribute to cellulose degradation [27]. In particular, GH5 and GH7 cellulases have been linked to fungal virulence, host colonization, and immune responses in the necrotroph *Sclerotinia sclerotiorum* [28], and the hemibiotrophs *Bipolaris sorokiniana* [29] and *Verticillium dahliae* [30]. These findings suggest that secreted GHs may function not only in carbohydrate degradation but also as effectors during plant pathogen interactions [31]. Also upregulated were AA9 lytic polysaccharide monooxygenases (LPMOs), formerly classified as GH61, which use copper to catalyze the oxidative cleavage of cellulose. AA9 proteins are upregulated during plant infection by necrotrophs such as *Botrytis cinerea* [32] and *Stagonosporopsis cucurbitacearum* [33] and may contribute to virulence through cell wall degradation.

Glycosyl hydrolases also degrade hemicellulose, a diverse group of polysaccharides that includes xylans, xyloglucans, and mannans. Fungal xylan degradation typically relies on endo-1,4-β-xylanases, mainly from GH10 and GH11, and β-xylosidases from GH3, GH43, and GH54 families [34]. Carbohydrate binding

modules can enhance GH activity e.g., removal of CBM91 module substantially reduced the ability of GH43 enzymes to hydrolyze xylan and xylo-oligosaccharides [35]. The GH10 and GH11 xylanases have also been implicated in fungal virulence [36]. In *Magnaporthe oryzae*, simultaneous silencing of multiple GH10 xylanase genes reduced host penetration, lesion development, and fungal spread [37]. Similarly, deletion of GH11 xylanase gene *xyn11A* in *B. cinerea* delayed lesion expansion and reduced lesion size by more than 70%, demonstrating its contribution to full virulence [38]. In *V. dahliae*, the secreted GH11 protein Vd424Y can enter the plant nucleus and induce cell death, suggesting that GH11 proteins have roles beyond xylan hydrolysis [39].

Pectin degrading glycosyl hydrolases including polygalacturonases, cooperate with pectate lyases (PL) and carbohydrate esterases (CE) to degrade and modify the galacturonic acid rich pectin matrix [40]. However, the disruption of GH28 endopolygalacturonases in *B. cinerea* [41] and *Aspergillus flavus* [42] reduces disease severity but does not eliminate pathogenicity [43]. In contrast, pectate lyase PL1 has been identified as a virulence factor required for full pathogenicity [44]. The CAZyme family CE5 cutinases are widely distributed across saprotrophic, biotrophic, and necrotrophic fungi [45, 46] although their contribution to pathogenicity varies among fungal species [47, 48]. In *T. ethacetica*, cutinase upregulation during wound-dependent infection may suggest a role in accessing plant lipids and cuticular waxes rather than initial penetration[46]. Overall, the extensive CAZyme response is consistent with extensive remodeling of host tissues that may increase access to host derived nutrients and facilitate hyphal growth.

The secreted protein repertoire provides a complementary means of interacting with the host beyond plant cell wall degradation. Cell death inducing proteins (CDIPs), including NLPs, CFEM-domain proteins, and CAZymes discussed above (GH7, GH11, GH28, PL1, and cutinases), may function as apoplastic effectors to influence host physiology, immune responses, and colonization through diverse mechanisms [49–51]. However, NLPs are not universally required for pathogenicity [52, 53], and typically induce cell death in dicots but not monocots [51]. CFEM-domain proteins have diverse roles, including iron homeostasis and host immune suppression [54, 55], although secretion signals and extracellular localization are important considerations when predicting effector function [56, 57]. The upregulation of the putative cytoplasmic effector BAS2, implicated in lifestyle transition of the hemibiotroph *Colletotrichum gloeosporioides* [58], is also intriguing. Functional studies are needed to establish whether these candidates contribute to host tissue degradation, defense modulation, nutrient acquisition, or other aspects of fungal growth. Their coordinated upregulation nevertheless provides a starting point for investigating how *T. ethacetica* interacts with palm tissue and how these processes compare to the better characterized necrotrophic pathogens.

Secreted aspartic proteases from several necrotrophic fungal pathogens can promote fungal virulence by degrading host proteins and disrupting plant defense responses [59, 60]. In *Cryphonectria parasitica*, for example, overexpression of peptidase A1 resulted in increased necrosis in chestnut bark and woody tissue [61]. Metalloproteases such as fungalysins can also counter host defense by cleaving plant chitinases, thereby protecting the fungal cell walls from degradation and facilitate infection [62, 63]. The

upregulation of aspartic proteases and multiple metalloprotease families, including three M36 fungalysins, in the present study therefore suggests a potential role in host defense evasion during *T. ethacetica* infection.

Transporters can shape plant pathogen interactions by mediating fungal metabolite export and the efflux of host-derived toxic compounds [64]. In *C. gloeosporioides*, oligopeptide transporters (OPTs) contribute to vegetative growth, conidial germination, oxidative stress response, cell wall integrity, and pathogenicity. Deletion of *CgOPT2* also downregulates genes encoding extracellular hydrolases, including cutinase, pectin lyase, and pectinesterase [65]. Transporter expression can also vary across infection stages, e.g., the high affinity hexose transporters CgHXT1 and CgHXT3 show increased expression during the biotrophic stage of *C. graminicola* infection that declines during necrotrophic growth [66]. Although additional infection timepoints are needed to resolve the roles of individual transporters in *T. ethacetica*, the concurrent upregulation of CAZymes and proteases together with sugar transporters and OPTs, suggests that extracellular degradation of host tissues is coupled to nutrient uptake.

Upregulation of a set of five collinear genes resembling a non-canonical isocyanide secondary metabolite biosynthetic gene cluster was observed. Isocyanides are implicated in both pathogenesis [67] and metal homeostasis [68]. The dual-domain isocyanide synthase-dioxygenase Dit1-TauD gene identified in this *T. ethacetica* cluster resembles the *Aspergillus fumigatus xan* gene involved in xanthocillin biosynthesis [69, 70]. Xanthocillin chelates copper and may provide competitive fitness advantage in copper depleted environments [70]. Copper predominantly occurs in protein bound forms in plant tissues [71]. During necrotrophic degradation, *T. ethacetica* may release copper from host proteins, including those associated with chloroplasts and mitochondria, increasing free copper availability and potentially promoting ROS production. The concurrent upregulation of the Dit1-TauD isocyanide cluster, and copper amine oxidase suggests potentially complementary roles in copper homeostasis and redox regulation. Copper amine oxidases can generate H_2O_2 during amine oxidation [72] that may promote ROS production, while fungal isocyanides can chelate copper [70] and potentially limit copper-driven oxidative stress. These putative activities may help shape redox balance during necrotrophic colonization but require functional validation.

Beyond copper homeostasis and redox regulation, the transcriptional response also implicates sulfur, iron, and phosphorus metabolism, suggesting broader adjustments in nutrient acquisition as colonization progresses. Together, these responses may reflect the capacity of *T. ethacetica* to regulate metal availability and exploit diverse nutrient sources within the heterogeneous environment of damaged host tissue. The coordinated expression of genes associated with tissue degradation, secreted host interacting proteins, proteolysis, and nutrient scavenging is characteristic of strategies employed by well-studied necrotrophic fungi.

Conclusions

This study characterized the transcriptional response of *Thielaviopsis ethacetica* and identified candidate genes and pathways potentially associated with palm colonization. Temporal expression patterns differed across sampling points, while enrichment analysis at 48 hpi highlighted translation, ribosome biogenesis, and carbohydrate metabolism, consistent with active fungal growth and host substrate utilization. Upregulated genes were also associated with plant cell wall degradation, oxidative carbohydrate processing, proteolysis, and nutrient acquisition. These findings suggest that host tissue degradation is linked to nutrient acquisition and utilization, consistent with a necrotrophic mode of colonization. The identification of 23 candidate effectors, including NPP1 and BAS2, three highly expressed DUF7029-containing proteins, and a putative isocyanide biosynthetic gene cluster provides candidates for further investigation of the *T. ethacetica* - palm interaction. Functional characterization of these genes, together with expanded temporal and experimental analyses, will be necessary to establish their specific contributions to host colonization and disease development.

Declarations

Research Funding

This study is supported by funding from USDA National Institute of Food and Agriculture Hatch project grant ID FLA-FTL-0066 available to BD, and USDA-ARS project 6038-13210-004-000-D available to MNR.

Ethics approval and consent to participate

Not applicable.

Consent for publication

Not applicable.

Competing interests

The authors declare no competing interests.

Author Contribution

BD designed and conceived the study. SC performed the experimental work. SuSap and BD performed data analysis, interpretation, and visualization. JR and NG contributed to data analysis. SuSap wrote the first draft. SuSin helped BD with supervision. MNR provided funding for sequencing. All authors read and approved the final manuscript.

Acknowledgement

This work is supported by the USDA National Institute of Food and Agriculture, Hatch project FLA-FTL-0066 and USDA-ARS under Project Number 6038-13210-004-000-D. Any opinions, findings, conclusions, or recommendations expressed in this publication are those of the author(s) and do not necessarily reflect the view of the National Institute of Food and Agriculture (NIFA) or the United States Department of Agriculture (USDA).

Data Availability

The sequencing data supporting this project are available at NCBI (www.ncbi.nlm.nih.gov) SRA under BioProject accession PRJNA1480769, and the RNAseq data are accessions SRX35878792 - SRX35878803. All other data supporting the conclusions of this article are included within the article and its supplementary information files.

References

1. Borges AF, de Alcântara Neto F, da Silva Matos K, Júnior JEAB, Júnior NSM, Moreira SI, et al. *Thielaviopsis ethacetica* the etiological agent of sugarcane pineapple sett rot disease in Brazil. Trop Plant Pathol. 2019;44:460–7. https://doi.org/10.1007/s40858-019-00298-9.
2. Álvarez E, Llano GA, Loke JB, Chacon MI. Characterization of *Thielaviopsis paradoxa* Isolates from Oil Palms in Colombia, Ecuador and Brazil. J Phytopathol. 2012;160:690–700. https://doi.org/10.1111/jph.12012.
3. Mbenoun M, Wingfield MJ, Begoude Boyogueno AD, Nsouga Amougou F, Petchayo Tigang S, Ten Hoopen GM, et al. Diversity and pathogenicity of the Ceratocystidaceae associated with cacao agroforests in Cameroon. Plant Pathol. 2016;65:64–78. https://doi.org/10.1111/ppa.12400.
4. Vo HH, Han V-C, Tran TT, Vu TT, Tran DK. First report of wilt and root rot on bell pepper (*Capsicum annuum*) caused by *Thielaviopsis ethacetica*. New Dis Rep. 2022;46:e12113. https://doi.org/10.1002/ndr2.12113.
5. Garofalo JF, Mcmillan RT. *Thielaviopsis* diseases of Palms. Proc Fla State Hortic Soc. 2004;117:324–5.
6. Streets RB. Heart Rot of the Date Palm Caused by *Thielaviopsis paradoxa* (DeSeynes) von Höhn. Technical Bulletin. Tucson, Arizona: University of Arizona Agricultural Experiment Station; 1933.
7. Elliott ML. *Thielaviopsis* Trunk Rot of Palm: PP-219/PP143, 1/2006. EDIS. 2019;2006. https://doi.org/10.32473/edis-pp143-2006
8. Cook MT. *Thielaviopsis paradoxa*; An important disease of Sugar Cane. J Agric Univ P R. 1932;16:205–11. https://doi.org/10.46429/jaupr.v16i2.15046
9. Ayika M-G, Rosano A, Valiente J, Chakrabarti S, Rollins JA, Dhillon B. Characterizing the Palm Pathogenic *Thielaviopsis* Species from Florida. J Fungi. 2024;10:247. https://doi.org/10.3390/jof10040247.

10. Ayika M-G, Bansal K, Chakrabarti S, Rosano A, Nageshwara-Rao M, Singh S, et al. Detached Leaf Assay for Palms Identifies Variable Disease Resistance to *Thielaviopsis* Species. Plant Dis. 2026;110:1867–74. https://doi.org/10.1094/PDIS-07-25-1577-RE.
11. Andrews S. FastQC A Quality Control Tool for High Throughput Sequence Data. 2010.
12. Chen S, Zhou Y, Chen Y, Gu J. fastp: an ultra-fast all-in-one FASTQ preprocessor. Bioinformatics. 2018;34:i884–90. https://doi.org/10.1093/bioinformatics/bty560.
13. Kim D, Paggi JM, Park C, Bennett C, Salzberg SL. Graph-based genome alignment and genotyping with HISAT2 and HISAT-genotype. Nat Biotechnol. 2019;37:907–15. https://doi.org/10.1038/s41587-019-0201-4.
14. Li H, Handsaker B, Wysoker A, Fennell T, Ruan J, Homer N, et al. The Sequence Alignment/Map format and SAMtools. Bioinformatics. 2009;25:2078–9. https://doi.org/10.1093/bioinformatics/btp352.
15. Pertea M, Pertea GM, Antonescu CM, Chang T-C, Mendell JT, Salzberg SL. StringTie enables improved reconstruction of a transcriptome from RNA-seq reads. Nat Biotechnol. 2015;33:290–5. https://doi.org/10.1038/nbt.3122.
16. R Core Team. R: A Language and Environment for Statistical Computing. Statistical software. Vienna, Austria: R Foundation for Statistical Computing; 2025.
17. Love MI, Huber W, Anders S. Moderated estimation of fold change and dispersion for RNA-seq data with DESeq2. Genome Biol. 2014;15:550. https://doi.org/10.1186/s13059-014-0550-8.
18. Wickham H, Vaughan D, Girlich M, tidyr. Tidy Messy Data. 2014. https://doi.org/10.32614/CRAN.package.tidyr. :1.3.2.
19. Wickham H, François R, Henry L, Müller K, Vaughan D. dplyr: A Grammar of Data Manipulation. 2014;:1.2.1. https://doi.org/10.32614/CRAN.package.dplyr.
20. Wickham H. Data Analysis. ggplot2. Cham: Springer International Publishing; 2016. pp. 189–201. https://doi.org/10.1007/978-3-319-24277-4_9.
21. Wilke CO, Wiernik BM. ggtext: Improved Text Rendering Support for ggplot2. 2020;:0.2.0. https://doi.org/10.32614/CRAN.package.ggtext
22. Slowikowski K. ggrepel: Automatically Position Non-Overlapping Text Labels with ggplot2. 2016;:0.9.8. https://doi.org/10.32614/CRAN.package.ggrepel
23. Kolde R. pheatmap: Pretty Heatmaps. R package. 2025.
24. Xu S, Hu E, Cai Y, Xie Z, Luo X, Zhan L, et al. Using clusterProfiler to characterize multiomics data. Nat Protoc. 2024;19:3292–320. https://doi.org/10.1038/s41596-024-01020-z.
25. Wickham H. httr: Tools for Working with URLs and HTTP.2012;:1.4.9. https://doi.org/10.32614/CRAN.package.httr
26. Ooms J. The jsonlite Package: A Practical and Consistent Mapping Between JSON Data and R Objects. 2014. https://doi.org/10.48550/arXiv.1403.2805

27. Lee GH, Min CW, Wang Y, Gupta R, Kim ST. Understanding the functional role of cell wall-degrading enzymes in *Magnaporthe oryzae* and their interactions with the rice immune system. Plant Physiol Biochem. 2026;231:111027. https://doi.org/10.1016/j.plaphy.2026.111027.
28. Liu X, Zhao H, Xie J, Fu Y, Li B, Yu X, et al. A Glycosyl Hydrolase 5 Family Protein Is Essential for Virulence of Necrotrophic Fungi and Can Suppress Plant Immunity. Int J Mol Sci. 2024;25:2693. https://doi.org/10.3390/ijms25052693.
29. Aich S, Singh RK, Kundu P, Pandey SP, Datta S. Genome-wide characterization of cellulases from the hemi-biotrophic plant pathogen, *Bipolaris sorokiniana*, reveals the presence of a highly stable GH7 endoglucanase. Biotechnol Biofuels. 2017;10:135. https://doi.org/10.1186/s13068-017-0822-0.
30. Lü J, Liu S, Zhou J, Feng Z, Wei F, Zhao L, et al. The glycoside hydrolase 7 member VdGH7a regulates *Verticillium dahliae* pathogenicity and induces host defenses by interacting with GhOLP1. J Integr Agric. 2025;24:4294–309. https://doi.org/10.1016/j.jia.2024.03.002.
31. Bradley EL, Ökmen B, Doehlemann G, Henrissat B, Bradshaw RE, Mesarich CH. Secreted Glycoside Hydrolase Proteins as Effectors and Invasion Patterns of Plant-Associated Fungi and Oomycetes. Front Plant Sci. 2022;13. https://doi.org/10.3389/fpls.2022.853106.
32. Blanco-Ulate B, Morales-Cruz A, Amrine KCH, Labavitch JM, Powell ALT, Cantu D. Genome-wide transcriptional profiling of *Botrytis cinerea* genes targeting plant cell walls during infections of different hosts. Front Plant Sci. 2014;5. https://doi.org/10.3389/fpls.2014.00435.
33. Guo M, Lou J, Han S, Li D, Song F. *Stagonosporopsis cucurbitacearum* Effector Protein ScAA9 Contributes to Virulence and Triggers Plant Immune Responses. Mol Plant Pathol. 2026;27:e70240. https://doi.org/10.1111/mpp.70240.
34. Kubicek CP, Starr TL, Glass NL. Plant Cell Wall–Degrading Enzymes and Their Secretion in Plant-Pathogenic Fungi. Annu Rev Phytopathol. 2014;52:427–51. https://doi.org/10.1146/annurev-phyto-102313-045831.
35. Pang SL, Wang YY, Wang L, Zhang XJ, Li YH. The CBM91 module enhances the activity of β-xylosidase/α-L-arabinofuranosidase PphXyl43B from *Paenibacillus physcomitrellae* XB by adopting a unique loop conformation at the top of the active pocket. Int J Biol Macromol. 2024;266:131275. https://doi.org/10.1016/j.ijbiomac.2024.131275.
36. Rafiei V, Vélëz H, Tzelepis G. The Role of Glycoside Hydrolases in Phytopathogenic Fungi and Oomycetes Virulence. Int J Mol Sci. 2021;22:9359. https://doi.org/10.3390/ijms22179359.
37. Nguyen QB, Itoh K, Van Vu B, Tosa Y, Nakayashiki H. Simultaneous silencing of endo-β-1,4 xylanase genes reveals their roles in the virulence of *Magnaporthe oryzae*. Mol Microbiol. 2011;81:1008–19. https://doi.org/10.1111/j.1365-2958.2011.07746.x.
38. Brito N, Espino JJ, González C. The Endo-β-1,4-Xylanase Xyn11A Is Required for Virulence in *Botrytis cinerea*. Mol Plant-Microbe Interactions®. 2006;19:25–32. https://doi.org/10.1094/MPMI-19-0025.
39. Liu L, Wang Z, Li J, Wang Y, Yuan J, Zhan J, et al. *Verticillium dahliae* secreted protein Vd424Y is required for full virulence, targets the nucleus of plant cells, and induces cell death. Mol Plant Pathol. 2021;22:1109–20. https://doi.org/10.1111/mpp.13100.

40. van den Brink J, de Vries RP. Fungal enzyme sets for plant polysaccharide degradation. Appl Microbiol Biotechnol. 2011;91:1477–92. https://doi.org/10.1007/s00253-011-3473-2.
41. Have AT, Mulder W, Visser J, Van Kan JAL. The Endopolygalacturonase Gene *Bcpg1* Is Required for Full Virulence of *Botrytis cinerea*. Mol Plant-Microbe Interactions®. 1998;11:1009–16. https://doi.org/10.1094/MPMI.1998.11.10.1009.
42. Shieh MT, Brown RL, Whitehead MP, Cary JW, Cotty PJ, Cleveland TE, et al. Molecular genetic evidence for the involvement of a specific polygalacturonase, P2c, in the invasion and spread of *Aspergillus flavus* in cotton bolls. Appl Environ Microbiol. 1997;63:3548–52. https://doi.org/10.1128/aem.63.9.3548-3552.1997.
43. Di Pietro A, Roncero MIG, Cloning. Expression, and Role in Pathogenicity of *pg1* Encoding the Major Extracellular Endopolygalacturonase of the Vascular Wilt Pathogen *Fusarium oxysporum*. Mol Plant-Microbe Interactions®. 1998;11:91–8. https://doi.org/10.1094/MPMI.1998.11.2.91.
44. Huertas-González MD, Ruiz-Roldán MC, García Maceira FI, Roncero MIG, Di Pietro A. Cloning and characterization of pl1 encoding an in planta-secreted pectate lyase of *Fusarium oxysporum*. Curr Genet. 1999;35:36–40. https://doi.org/10.1007/s002940050430.
45. Lee M-H, Chiu C-M, Roubtsova T, Chou C-M, Bostock RM. Overexpression of a Redox-Regulated Cutinase Gene, *MfCUT1*, Increases Virulence of the Brown Rot Pathogen *Monilinia fructicola* on *Prunus* spp. Mol Plant-Microbe Interact. 2010;23:176–86. https://doi.org/10.1094/MPMI-23-2-0176.
46. Arya GC, Cohen H. The Multifaceted Roles of Fungal Cutinases during Infection. J Fungi. 2022;8:199. https://doi.org/10.3390/jof8020199.
47. Sweigard JA, Chumley FG, Valent B. Disruption of a *Magnaporthe grisea* cutinase gene. Mol Gen Genet. 1992;232:183–90.
48. Stahl DJ, Schäfer W. Cutinase is not required for fungal pathogenicity on pea. Plant Cell. 1992;4:621–9. https://doi.org/10.1105/tpc.4.6.621.
49. De Wit PJGM, Mehrabi R, Van Den Burg HA, Stergiopoulos I. Fungal effector proteins: past, present and future. Mol Plant Pathol. 2009;10:735–47. https://doi.org/10.1111/j.1364-3703.2009.00591.x.
50. Qutob D, Kemmerling B, Brunner F, Küfner I, Engelhardt S, Gust AA, et al. Phytotoxicity and Innate Immune Responses Induced by Nep1-Like Proteins. Plant Cell. 2007;18:3721–44. https://doi.org/10.1105/tpc.106.044180.
51. Li Y, Han Y, Qu M, Chen J, Chen X, Geng X, et al. Apoplastic Cell Death-Inducing Proteins of Filamentous Plant Pathogens: Roles in Plant-Pathogen Interactions. Front Genet. 2020;11:661. https://doi.org/10.3389/fgene.2020.00661.
52. Zhou B-J, Jia P-S, Gao F, Guo H-S. Molecular Characterization and Functional Analysis of a Necrosis- and Ethylene-Inducing, Protein-Encoding Gene Family from *Verticillium dahliae*. Mol Plant Microbe Interact. 2012;25:964–75. https://doi.org/10.1094/MPMI-12-11-0319.
53. Motteram J, Küfner I, Deller S, Brunner F, Hammond-Kosack KE, Nürnberger T, et al. Molecular Characterization and Functional Analysis of MgNLP, the Sole NPP1 Domain–Containing Protein,

from the Fungal Wheat Leaf Pathogen *Mycosphaerella graminicola*. Mol Plant Microbe Interact. 2009;22:790–9. https://doi.org/10.1094/MPMI-22-7-0790.

54. Wang D, Zhang D-D, Song J, Li J-J, Wang J, Li R, et al. *Verticillium dahliae* CFEM proteins manipulate host immunity and differentially contribute to virulence. BMC Biol. 2022;20:55. https://doi.org/10.1186/s12915-022-01254-x.
55. Hong T, Wang S, Luo Z, Ren Q, Wu D, Wang L, et al. *Fusarium sacchari* CFEM Proteins Suppress Host Immunity and Differentially Contribute to Virulence. Int J Mol Sci. 2024;25:12805. https://doi.org/10.3390/ijms252312805.
56. Chen S, Songkumarn P, Venu RC, Gowda M, Bellizzi M, Hu J, et al. Identification and Characterization of In planta–Expressed Secreted Effector Proteins from *Magnaporthe oryzae* That Induce Cell Death in Rice. Mol Plant-Microbe Interactions®. 2013;26:191–202. https://doi.org/10.1094/MPMI-05-12-0117-R.
57. Guo X, Zhong D, Xie W, He Y, Zheng Y, Lin Y, et al. Functional Identification of Novel Cell Death-inducing Effector Proteins from *Magnaporthe oryzae*. Rice. 2019;12:59. https://doi.org/10.1186/s12284-019-0312-z.
58. An B, Wang W, Guo Y, Wang Q, Luo H, He C. BAS2 Is Required for Conidiation and Pathogenicity of *Colletotrichum gloeosporioides* from Hevea brasiliensis. Int J Mol Sci. 2018;19:1860. https://doi.org/10.3390/ijms19071860.
59. Movahedi S, Heale JB. The roles of aspartic proteinase and endo-pectin lyase enzymes in the primary stages of infection and pathogenesis of various host tissues by different isolates of *Botrytis cinerea* Pers ex. Pers Physiol Mol Plant Pathol. 1990;36:303–24. https://doi.org/10.1016/0885-5765(90)90061-2.
60. Wang C, Zheng Y, Liu Z, Qian Y, Li Y, Yang L, et al. The secreted FolAsp aspartic protease facilitates the virulence of *Fusarium oxysporum* f. sp. *lycopersici*. Front Microbiol. 2023;14:1103418. https://doi.org/10.3389/fmicb.2023.1103418.
61. Figueiredo L, Santos RB, Figueiredo A. Defense and Offense Strategies: The Role of Aspartic Proteases in Plant–Pathogen Interactions. Biology. 2021;10:75. https://doi.org/10.3390/biology10020075.
62. Guo F, Pan L, Liu H, Lv L, Chen X, Liu Y, et al. Whole-Genome Metalloproteases in the Wheat Sharp Eyespot Pathogen *Rhizoctonia cerealis* and a Role in Fungal Virulence. Int J Mol Sci. 2022;23:10691. https://doi.org/10.3390/ijms231810691.
63. Wang X, He M, Liu H, Ding H, Liu K, Li Y, et al. Functional Characterization of the M36 Metalloprotease FgFly1 in *Fusarium graminearum*. J Fungi. 2022;8:726. https://doi.org/10.3390/jof8070726.
64. Del Sorbo G, Schoonbeek H, De Waard MA. Fungal Transporters Involved in Efflux of Natural Toxic Compounds and Fungicides. Fungal Genet Biol. 2000;30:1–15. https://doi.org/10.1006/fgbi.2000.1206.

65. Li X, Liu S, Zhang N, Liu Z. Function and transcriptome analysis of an oligopeptide transporter CgOPT2 in the rubber anthracnose fungus *Colletotrichum gloeosporioides*. Physiol Mol Plant Pathol. 2021;115:101661. https://doi.org/10.1016/j.pmpp.2021.101661.
66. Lingner U, Münch S, Deising HB, Sauer N. Hexose Transporters of a Hemibiotrophic Plant Pathogen: Functional variations and regulatory differences at different stages of infection. J Biol Chem. 2011;286:20913–22. https://doi.org/10.1074/jbc.M110.213678.
67. Gloer JB, Poch GK, Short DM, McCloskey DV. Structure of brassicicolin A: a novel isocyanide antibiotic from the phylloplane fungus *Alternaria brassicicola*. J Org Chem. 1988;53:3758–61. https://doi.org/10.1021/jo00251a017.
68. Raffa N, Won TH, Sukowaty A, Candor K, Cui C, Halder S, et al. Dual-purpose isocyanides produced by *Aspergillus fumigatus* contribute to cellular copper sufficiency and exhibit antimicrobial activity. Proc Natl Acad Sci. 2021;118:e2015224118. https://doi.org/10.1073/pnas.2015224118.
69. Lim FY, Won TH, Raffa N, Baccile JA, Wisecaver J, Rokas A, et al. Fungal Isocyanide Synthases and Xanthocillin Biosynthesis in *Aspergillus fumigatus*. mBio. 2018;9:e00785–18. https://doi.org/10.1128/mBio.00785-18.
70. Raffa N, Won TH, Sukowaty A, Candor K, Cui C, Halder S, et al. Dual-purpose isocyanides produced by *Aspergillus fumigatus* contribute to cellular copper sufficiency and exhibit antimicrobial activity. Proc Natl Acad Sci. 2021;118:e2015224118. https://doi.org/10.1073/pnas.2015224118.
71. Rae TD, Schmidt PJ, Pufahl RA, Culotta VC, O'Halloran V. Undetectable Intracellular Free Copper: The Requirement of a Copper Chaperone for Superoxide Dismutase. Science. 1999;284:805–8. https://doi.org/10.1126/science.284.5415.805.
72. Svoboda T, Beltran E, Spörhase P, Fruhmann P, Bartholomäus A, Wiesenberger G, et al. The fungal pathogen *Fusarium graminearum* can hydrolyse typtamine-derived hydroxy-cinnamic acid amide defence compounds, and generates highly increased auxin levels in wheat via Copper Amine-Oxidases. Mol Plant Pathol. 2026;27:e70325. https://doi.org/10.1111/mpp.70325.

Figures

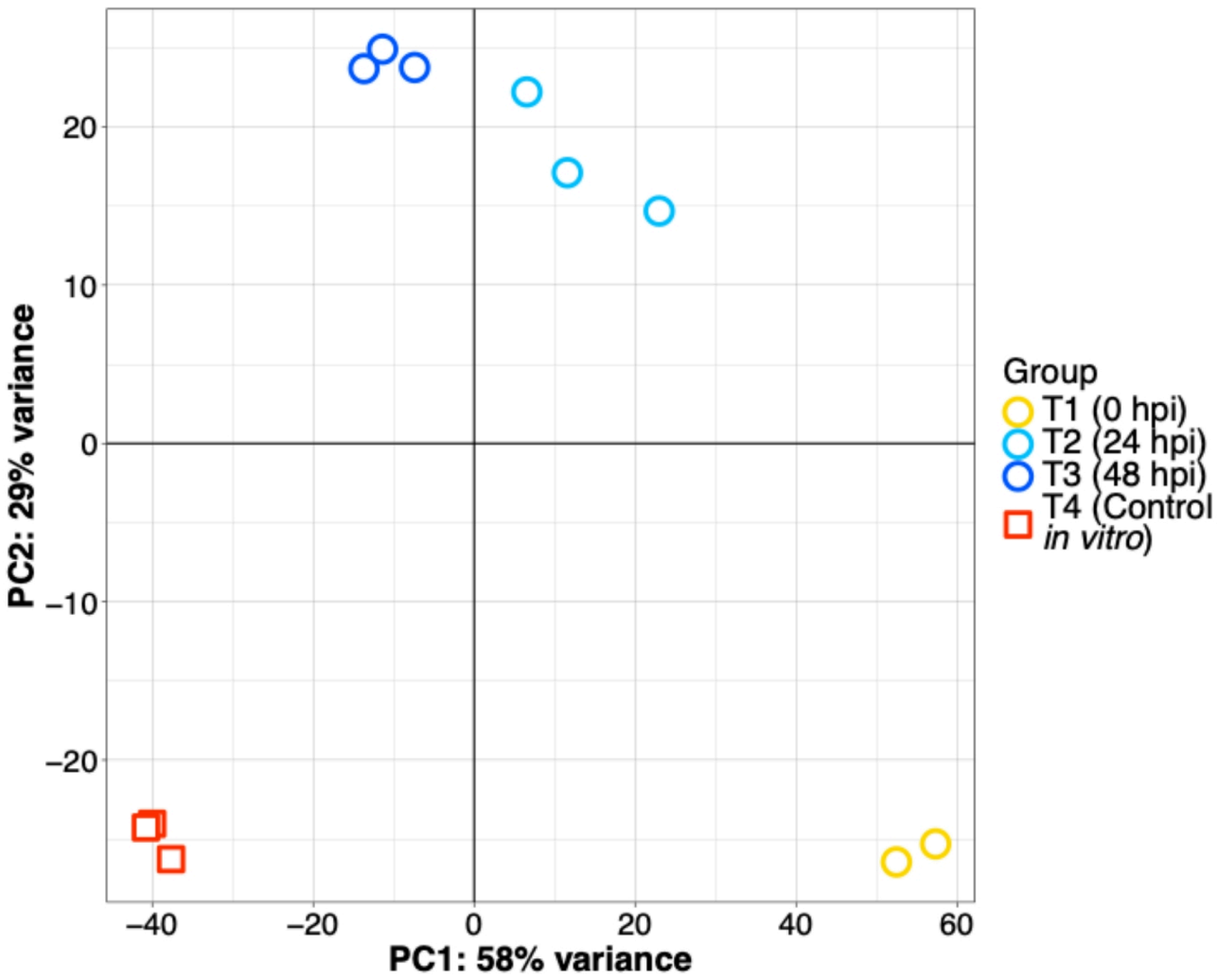

Figure 1

Principal component analysis (PCA) of gene expression profiles across eleven *Thielaviopsis ethacetica* samples. Each point represents an individual sample, with colors and shapes indicating experimental groups, T1 (0 hours post inoculation (hpi); ungerminated spores), T2 (24 hpi; early germination and host colonization), T3 (48 hpi; active necrotic lesion formation), and T4 (48 h *in vitro* grown mycelia). The percentages of variance explained by the first (PC1) and second (PC2) principal components are indicated on the respective axes. Prior to PCA, normalized read counts were transformed using the variance stabilizing transformation (vst) implemented in DESeq2. PCA was performed using 500 genes with the highest variance across samples.

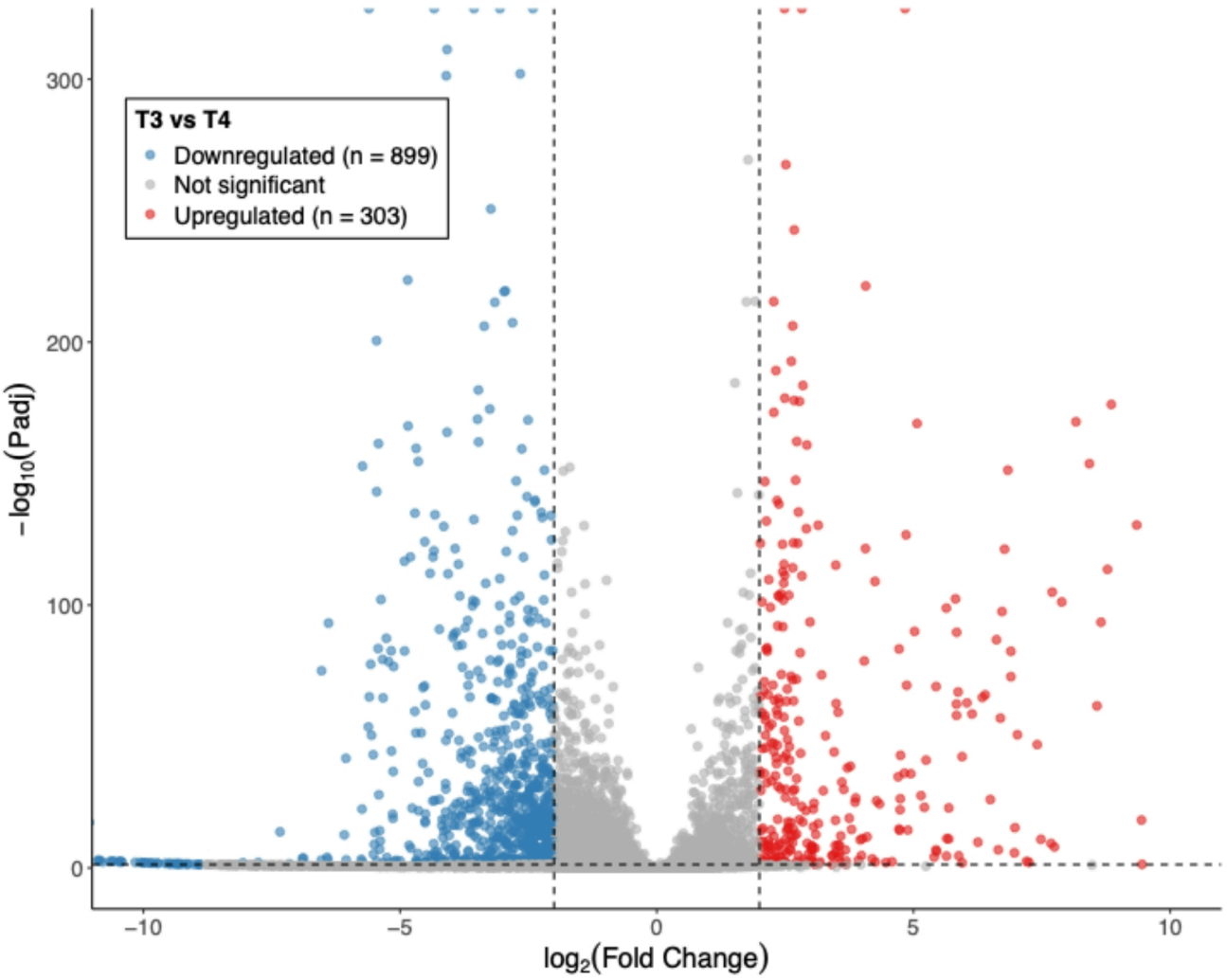

Figure 2

Volcano plot of differential gene expression in *Thielaviopsis ethacetica* at 48 hours post inoculation (hpi) compared with *in vitro* control (T3 vs T4). Each dot represents a gene, and genes with an absolute $\log_2$ fold change ≥ 2 and an adjusted *P* value ≤ 0.05 were considered to be significantly differentially expressed. Red and blue dots represent significantly up- and down-regulated genes, respectively, whereas genes not meeting both significance criteria are shown in gray. Dashed vertical lines indicate $\log_2$ fold change values of -2 and +2, and dashed horizontal line indicates an *P*adj value of 0.05. Numbers of up- and downregulated genes are indicated in the legend.

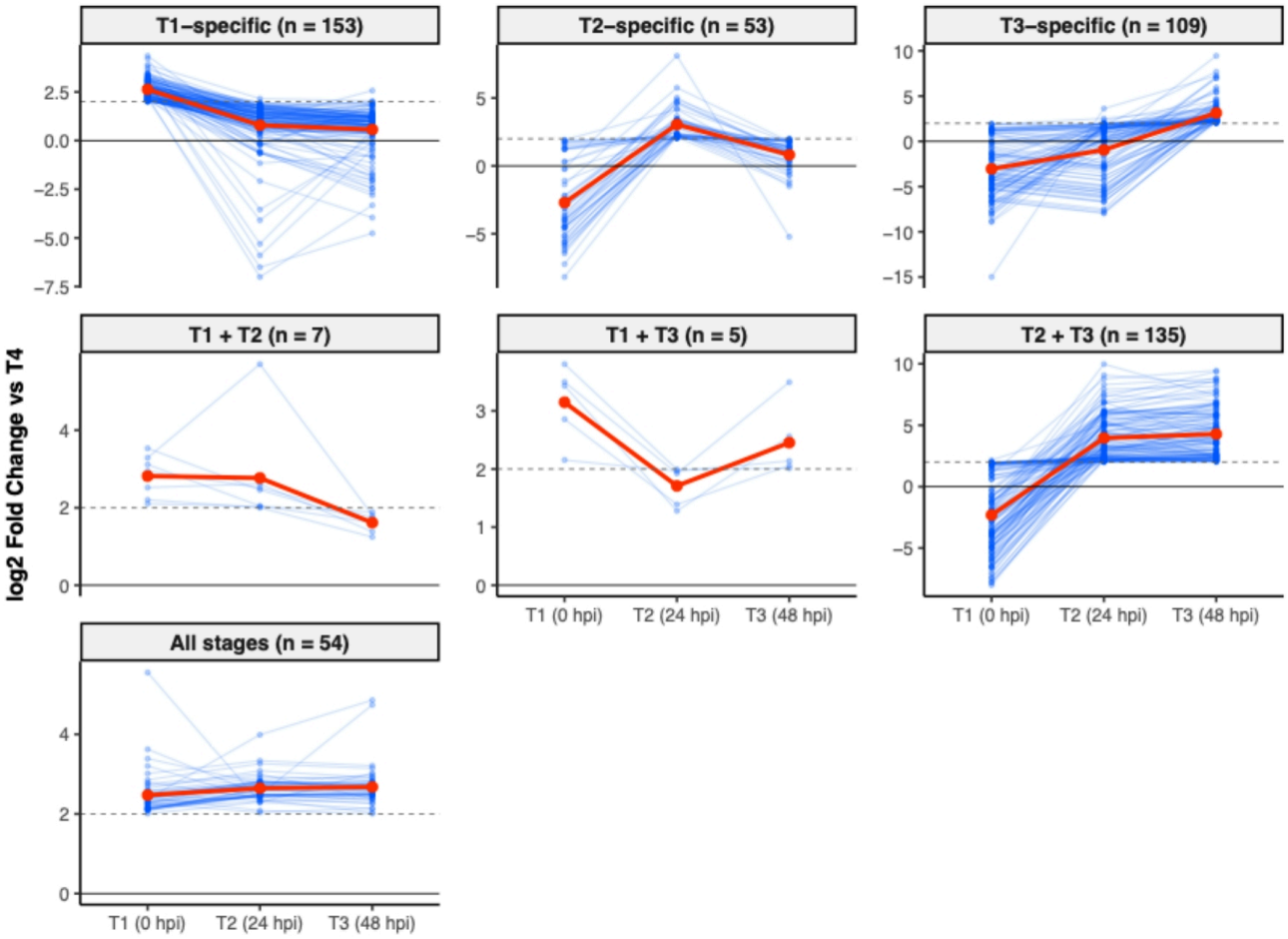

Figure 3

Temporal gene expression profiles during *Thielaviopsis ethacetica* infection. Genes classified according to significant upregulation at 0 h (T1), 24 h (T2), and 48 h (T3) relative to *in vitro* control (T4). Expression patterns included genes upregulated at a single time point, at two time points, or at all three time points. Significant upregulation was defined as log2FC ≥ 2 and *P*adj ≤ 0.05. Blues lines and points represent individual gene expression profiles, whereas red line and points indicate mean $\log_2$ fold change for each expression pattern at each time point. The solid horizontal line indicates $\log_2$ fold change of zero, and the dashed horizontal line indicates the expression threshold i.e., $\log_2$ fold change = 2. Each panel represents a distinct expression pattern, with the number of genes indicated in panel heading. The y-axis scales differ among panels.

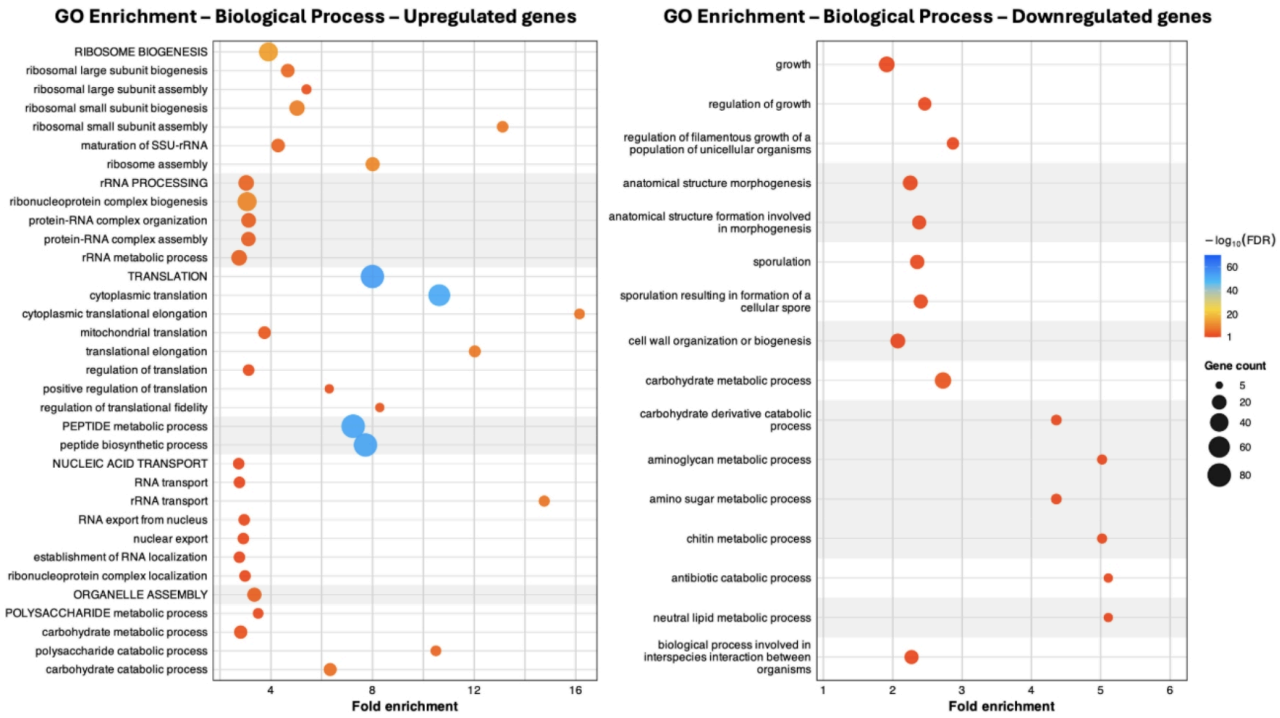

Figure 4

Gene Ontology (GO) biological process enrichment analysis of up- and downregulated genes in *Thielaviopsis ethacetica* at 48 h post inoculation (T3 vs T4). Over representation analysis (ORA) was performed separately for A) upregulated genes and B) downregulated genes. The x-axis represents fold enrichment, point size indicates the number of genes associated with each GO term, and point color represents the enrichment significance. Enriched GO terms were identified using a *P*adj value cutoff of 0.05. The same color and point size scales were used in both panels to facilitate comparison.

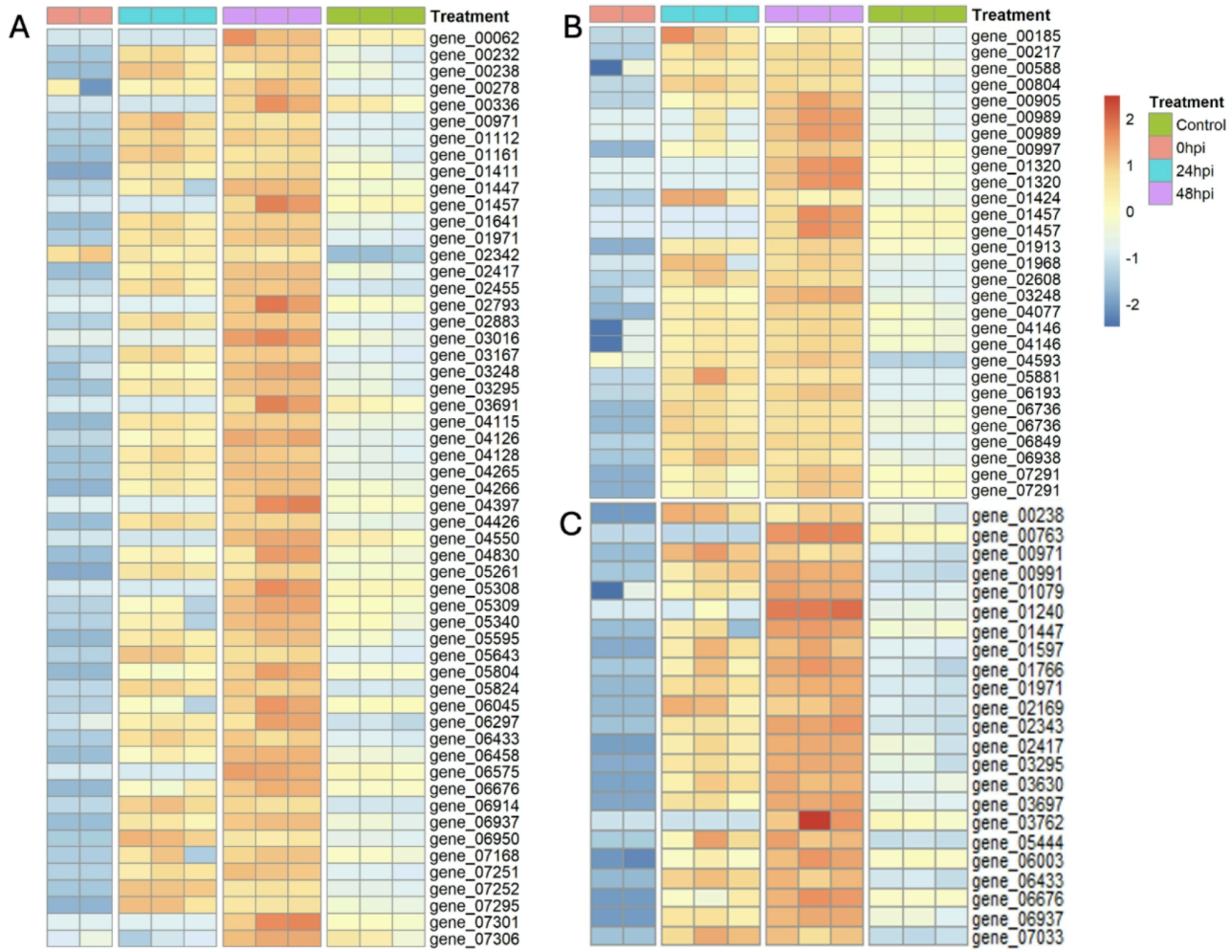

Figure 5

Heatmap for upregulated genes at 48 hpi (T3 vs T4). Differentially expressed genes are grouped into three functional categories, A) carbohydrate active enzymes (CAZymes), B) peptidases, and C) candidate effectors. Gene expression levels are represented as Z-scores calculated from normalized expression values across samples, with red and blue representing high and low expression, respectively.

Supplementary Files

This is a list of supplementary files associated with this preprint. Click to download.

- Fig.S2.png
- Fig.S1.png
- supplementalTables.xlsx